Automatic Detection of Sulcal Bottom Lines in MR Images of the Human Brain

Gabriele Lohmann, Frithjof Kruggel, D. Yves von Cramon

Max-Planck-Institute of Cognitive Neuroscience, Inselstr. 22-26
04103 Leipzig, Germany
e-mail: {lohmann,kruggel}@cns.mpg.de

Abstract. This paper describes an automatic procedure for extracting sulcal bottom lines from MR (magnetic resonance) images of the human brain, which will serve as a tool for landmark extraction as well as for investigating the morphometry of sulci. The procedure consists of a sequence of several image processing steps, including morphological operators and a constrained distance transform which provides information about sulcal depth at each location.

1 Introduction

This paper describes an automatic procedure for extracting the bottom lines of the main cortical sulci from MR (magnetic resonance) images of the human brain. The sulci are deep narrow valleys or folds of the cortical surface.

The automatic detection of sulcal bottom lines is of interest for several reasons. Firstly, sulcal bottom lines are suited to serve as landmarks that can be used to reference brain locations in a way that is anatomically meaningful. Secondly, sulcal bottom lines allow us to represent an entire sulcus by a tree like structure of curves rather than of surfaces, and thus present a highly condensed representation of a prominent landmark.

Another aspect associated with the work reported here is that in the process of the extraction of sulcal bottom lines information about sulcal depth becomes available. This aspect may be relevant in studying interpersonal sulcal variability. It is, for instance, an ongoing question whether the interpersonal variability in sulcal patterns decreases with depth. The depth information made available by our method will hopefully help to address this issue from a new viewpoint.

Previous investigations of sulcal structure and interpersonal variability [1], [2], [3] were often based on manual segmentations and were therefore restricted to very few data sets. Automatic procedures for the identification of sulcal bottom lines have not been reported in the literature so far.

However, the automatic extraction of other prominent lines as landmarks from 3D data sets has received considerable attention. Particularly, the computation of curvature properties for the purpose of ridge line extraction should be mentioned. The methods described in [4],[5],[6],[7] fall into that category. Our approach differs in that it extracts lines of *maximal depth* as measured from the smoothed brain surface as opposed to lines of *maximal curvature*. Sulcal bottom

lines do not usually coincide with lines of maximal curvature, so that ridge line extraction is not a viable approach to our problem.

The automatic extraction of sulcal structures has been the subject of several research projects either focusing on the extraction of sulcal skeletons [8] or sulcal surfaces [9],[10]. These techniques differ from ours in that they are not aimed at making depth information available.

Our bottom line extraction process consists of several steps beginning with a segmentation procedure to identify the sulcal interiors. We skeletonize the sulcal compartments to obtain medial surfaces which are then eroded until the bottom is reached. Finally, the resulting chains of bottom voxels are connected into a graph of polygons. In the following, each of these steps will be described in detail. The method reported here is an extension of our earlier work [11] improving it in both accuracy and computational efficiency.

2 Depth measurements

We start out with a white matter segmentation of the initial MR data set. To obtain the sulcus interior, we apply a 3D morphological closing filter using a sphere shaped structuring element of very large size, e.g. of radius 7 or larger. The difference between the binarized white matter image and the morphologically closed image yields the sulcal areas.

Once sulcal and white matter areas are labelled, depth measurements in the sulcal compartments are made. The technique used for this purpose is an adaptation of the constrained distance transform [12]. Each voxel which has been labelled as "sulcus interior" receives a depth label indicating its depth as measured from the idealized brain surface.

Standard distance transforms [13] require a binary image as input in which feature points are marked as "white" pixels. In the distance transformed image each "black" voxel receives a label indicating its distance from the nearest feature point.

Input images to constrained distance transforms may contain an additional third type of label which represent a class of "obstacle" points. The constrained distance transform attributes a distance label to each "black" voxel towards its nearest "white" voxel where the length is measured along paths that are forced to avoid voxels labelled as "obstacles". In the present case, the obstacle voxels are the ones that are labelled as "white matter". We now seek the lengths of shortest paths from each sulcal voxel towards the idealized surface which do not trespass white matter areas.

The distance transform is performed by moving two 3D filter masks over the image in two separate scans. The filter mask represents local distances which are propagated through the entire image as the algorithm progresses. Note that some voxels may be entirely surrounded by obstacle voxels so that no valid path to any feature voxel exists. Those voxels will of course remain unlabeled.

Shallow sulci can be eliminated by thresholding the output of the depth labeling procedure. Typically, we are only interested in sulci deeper than 4mm.

3 Extraction of sulcal medial surfaces

After the sulcal compartments have been identified, their medial surface is extracted. A large number of skeletonization algorithms have been reported in the literature, e.g. [14], [15],[16]. In our experiments we found that a modified version of Tsao's method [16] yielded the best results.

Tsao's algorithm performs a parallel deletion of directional border points where a voxel is a border voxel in a given principal direction (north, south, west, east, top, bottom) if its neighbour in that direction belongs to the background.

We modified this algorithm by changing the order in which points are considered for deletion. The basic idea[17] is the following: we first compute the distance transform of the image to be thinned such that each foreground voxel receives a label indicating its distance from the nearest background voxel. We then place all foreground voxels in an array and sort it by distance values. The points that receive the smallest distance values are the first to be considered for deletion, where the same deletion criteria and subcycle schedule as in Tsao's original algorithm is used. If no more points at this distance level can be deleted, we move on to the next higher distance value, and so on until all distance levels have been processed.

There are two prime advantages of this method over the original procedure. Firstly, by placing all foreground voxels into an array we do not need to scan the entire image for each deletion subcycle, and thus gain a considerable increase in computation speed. Secondly, by sorting this array according to distance values, we achieve a much better localization for the resulting skeleton as skeletal voxels are forced to reside on local maxima of the distance transform. Figure 1 shows two slices of a thinning result.

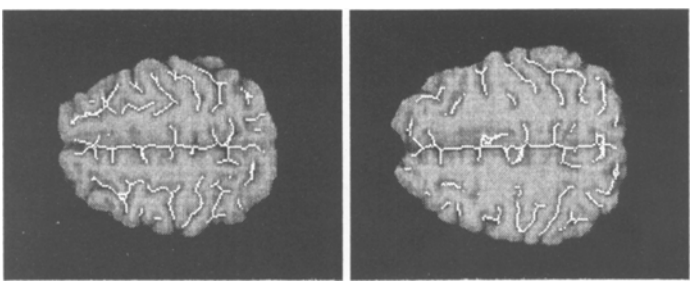

Figure 1: 3D Thinning: axial slices

4 Extraction of sulcal bottom lines

The next step consists in reducing the medial surface such that only its bottom line remains. We use a modification of the thinning algorithm to achieve this. The basic idea is to remove voxels at progressively deeper levels while leaving voxels at the sulcus ends unchanged.

As before, we place all foreground voxels belonging to the medial surface into an array. Note that each voxel in this array already has a depth label obtained

in a previous step. We now use this labeling to sort the array by depth and begin by deleting voxels at the smallest depth level. Points are deletable if they are topologically simple, and if they are not endpoints, where end points are characterized by the fact that there are no more than two non-zero 26-adjacent voxels.

In contrast to our thinning procedure, deletion is now performed sequentially rather than in parallel as only sequential deletion is guaranteed to preserve topology. A pseudo-code version of the algorithm is given below:

```
BottomLine(image)
{
  copy medial surface voxels into array;
  sort array by depth;
  for (depth d = 1 to maxdepth) {
    ndelete = 1;
    while (ndelete > 0) {
      ndelete = 0;
      for (all voxels v in array at depth d) {
        if (not EndVoxel(v) and SimplePoint(v)) {
          Delete(v);
          ndelete = ndelete + 1;
      }
    }
  }
}
```

The above procedure reduces sulcal medial surfaces to sulcus bottom lines so that at the end of this stage only one-voxel thick chains of foreground voxels remain.

We now transfer the binary raster image into a graph structure by first creating a node for each foreground voxel specifying its voxel address and its depth. We then establish links between nodes such that each node is connected to all its 26-adjacent neighbouring nodes. We thus obtain an undirected graph with a symmetric arc relation where adjacent nodes are linked in both directions. Lastly, spurious branches are pruned in a final postprocessing step.

5 Experiments

The method was applied to seven T1 weighted MRI data sets from three different MR scanners. The same set of parameters was used for all data sets. The results were checked manually by two human experts (neurologists) doing random checks. The results were found to be correct in almost every case. The only errors that were found are related to the following systematic problem.

The algorithm blindly interprets every cavity or indentation within the white matter as a sulcus. Therefore, structures such as the basal ganglia and the ventricles are filled with a "sulcus" line unless those structures have been masked

out beforehand. For the same reason, the Cisterna pontis and Cisterna vallecula cerebri are also wrongly interpreted as "sulci" causing a conglomeration of lines around the brain basis connecting the two hemispheres. In our experiments, we used a visual editor to manually break and remove such obviously incorrect lines. With the exception of those systematic errors, the results were found to be correct.

Figure 2 shows some bottom lines resulting from one such experiment, indicating how the verification was done: the mouse cursor is linked to the sagittal, coronal and axial slices of the data set so that a mouse click onto a node in the graph automatically positions the cursor to the corresponding location in the MR data set, so that the expert can assess the correctness of the location of a node.

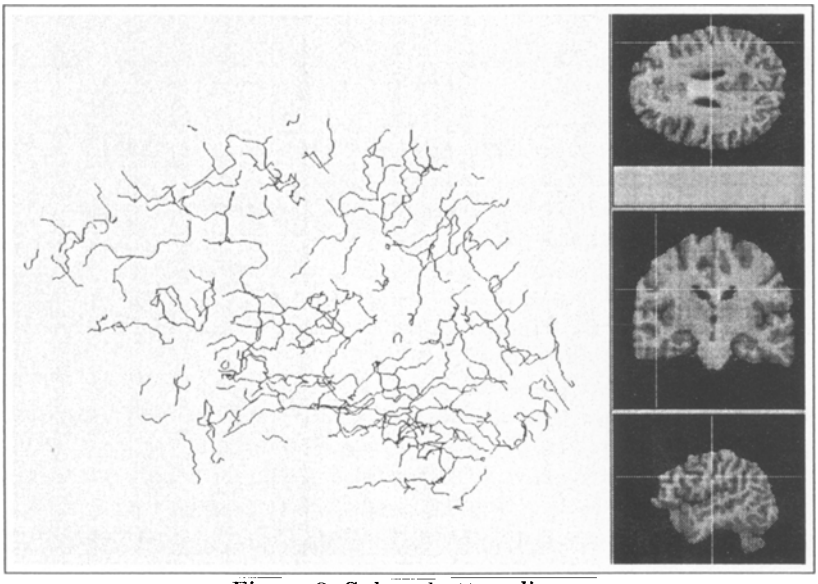

Figure 2: Sulcus bottom lines

6 Conclusion

A new method for the extraction of sulcal bottom lines was presented. The method is essentially parameter free with the exception of two thresholding parameters for the postprocessing step and another threshold applied to the depth labelled image to exclude shallow sulci. All three thresholds are uncritical in the sense that standard settings can be adopted.

Our method will serve both as a tool for landmark extraction as well as a tool for investigating the morphometry of sulci. Future work will focus on a classification of sulcus types and on studying interpersonal variability of sulcal structures. The depth information provided by this tool will play a central role in this work. In particular, we hope that this method will help to clarify to question of whether or not interpersonal variability decreases with depth.

References

1. M. Ono, S. Kubik, C.D. Abernathy. *Atlas of the cerebral sulci.* Georg Thieme Verlag, Stuttgart, New York, 1990.
2. T. Paus, F. Tomaiuolo, N. Otaky, D. MacDonald, M. Petrides, J. Atlas, R. Morris, A.C. Evans. Human cingulate and paracingulate sulci: pattern, variability, asymmetry, and probabilistic map. *Cerebral Cortex*, 6:207–214, Mar/Apr 1996.
3. P.M. Thompson, C.Schwartz, R.T. Lin, A.A. Khan, A.T. Toga. Three-dimensional statistical analysis of sulcal variability in the human brain. *The Journal of Neuroscience*, 16(13):4261–4274, 1996.
4. J. Declerck, G. Subsol, J.-P. Thirion, N. Ayache. Automatic retrieval of anatomical structures in 3D medical images. In N. Ayache, editor, *Computer Vision, Virtual Reality and Robotics in Medicine*, pages 153–162, Nice, France, April 1995. Springer Lecture Notes, 905.
5. A. Guéziec, N. Ayache. Smoothing and matching of 3-d space curves. *International Journal of Computer Vision*, 12(1):79–104, 1994.
6. O. Monga, S. Benayoun. Using partial derivatives of 3d images to extract typical surface features. *Computer vision and image understanding*, 61(2):171–189, March 1995.
7. J.P. Thirion, A. Gourdon. The marching lines algorithm: new results and proofs. *Technical Report No. 1881*, April 1993.
8. R.L. Ogniewicz, G. Szekely, O. Kübler. Detection of prominent boundary points based on structural characteristics of the hierarchic medial axis transform. In H. (Hrsg.) Pöppl, S. H.; Handels, editor, *15. DAGM-Symposium, Mustererkennung 1993*, pages 321–331. Springer Verlag, 1993.
9. Yaorong Ge, J.Michael Fitzgerald, Benoit M. Dawant, Jun Bao, Robert M. Kessler, Richard A. Margolin. Accurate localization of cortical convolutions in MR brain images. *IEEE Transactions on Medical Imaging*, 15(4):418–428, Aug. 1996.
10. M. Valliant, C. Davatzikos, R.N. Bryan. Finding 3D parametric representations of the deep cortical folds. In *Proc. Mathematical Methods in biomedical image analysis (MMBIA 96)*, pages 151–157, San Francisco, CA, June 1996. IEEE Computer Society.
11. G. Lohmann, F. Kruggel. Extracting lines of maximal depth from MRI images of the human brain. In *Proc. Intern. Conf. on Pattern Recognition*, Wien, Aug. 1996.
12. P.W.Verbeek, L. Dorst, B.J.H.Verwer, F.C.A. Groen. Collision avoidance and path finding through constrained distance transformation in robot state space. In *Proc. Intelligent Autonomous Systems*, pages 634–641, Amsterdam, The Netherlands, Dec. 1986.
13. G. Borgefors. Distance transforms in arbitrary dimensions. *Computer Vision, Graphics, and Image Processing*, 27:321–345, 1984.
14. T.C.Lee, R.L.Kashyap, C.N. Chu. Building skeleton models via 3-d medial surface axis thinning algorithms. *Computer Vision, Graphics, and Image Processing*, 56(6):462–478, 1994.
15. R.L. Ogniewicz, M. Ilg. Voronoi skeletons: theory and applications. In *Proc. Computer Vision and Pattern Recognition (CVPR 92)*, pages 63–69. Computer Society Press, 1992.
16. Y.F. Tsao, K.S. Fu. A parallel thinning algorithm for 3d pictures. *Computer Graphics Image Proc.*, 17:315–331, 1981.
17. G. Malandain. personal communication, July 1996.